Received: 23 October 2023 | Revised: 3 April 2024 | Accepted: 3 April 2024

DOI: 10.1002/appl.202300105

Applied Research

RESEARCH ARTICLE

Integration and characterization of a zeolite material in a microcomponent for measurements of environmental carbon dioxide

Erika Åkerfeldt | **Greger Thornell** | **Anders Persson**

Department of Materials Science and Engineering, Uppsala University, Uppsala, Sweden

Correspondence
Erika Åkerfeldt, Department of Materials Science and Engineering, Uppsala University, Uppsala, Sweden.
Email: erika.akerfeldt@angstrom.uu.se

Funding information
Svenska Forskningsrådet Formas

Abstract

This study demonstrates integration of a zeolite material in a ceramic microcomponent intended for use in sampling and analysis of environmental carbon dioxide (CO_2). The zeolite material was integrated in bulk form, allowing for adsorption of large quantities of CO_2 compared to previous integration attempts as thin films. To obtain a porous bulk material, an injectable slurry was developed, where expandable polymeric microspheres were added as a sacrificial template. By varying water and sphere contents of the slurry, it was possible to tune the porosity of the zeolite material between 55% and 72%. This in turn affected the flow resistance of the microcomponents, where an increase in the porosity of the filling from 62% to 72% reduced the flow resistance from 84 to 28 kPa min cm^{-3}. In addition, the spheres facilitated complete fillings free from cracks. The zeolite material was seen to retain its ability to adsorb CO_2 after processing, but it was not possible to quantify the level of retention compared to unprocessed zeolite.

KEYWORDS
carbon dioxide adsorption, expandable microspheres, greenhouse gas measurement, microsystems technology, zeolite 13X

INTRODUCTION

Mapping of the global carbon cycle is important for our ability to understand anthropogenic climate change and to implement suitable policies and actions to mitigate it. However, even though our knowledge increases continuously, the current picture of the global carbon cycle still suffers from large uncertainties [1, 2]. One reason is that the data available is still limited, both geospatially, as well as to measurements of carbon dioxide (CO_2) concentrations and fluxes in and between soils, waters and the atmosphere.

Part of the cause for the scarcity of available data can likely be attributed to difficulties in conducting the necessary measurements, where manual sampling methods are laborious [3] and the instrumentation needed for automatic sampling is expensive [2, 3]. Furthermore, the sampling sites are often remote, making transportation of equipment challenging, and access to electricity and remote communication limited. To make measurements of environmental CO_2 simpler, less expensive, and hence more available, this study proposes the use of microsystems technology (MST). In MST, the inherent reduction of size offers reductions in manufacturing cost and power consumption, as well as an increase in mobility, as mentioned by Zhou et al., [4] who also provide a general introduction to MST.

The approach suggested here consists of a microfluidic platform, where a liquid or gaseous sample is collected, and from which CO_2 is separated and retained for subsequent analysis in a microplasma

spectrometer [5]. This study focuses on the sample handling part of the platform, where CO_2 is to be separated, enriched to quantifiable levels, and retained for subsequent measurements. One possible way to achieve this is to use adsorbents, which then need to be integrated into the microsystem.

One category of CO_2 adsorbent materials is zeolites [6]. The adsorption capacity of zeolites varies with temperature and pressure, so that the CO_2 that is adsorbed under atmospheric conditions can be desorbed by either increasing the temperature or decreasing the pressure. Zeolites are commonly used at the macroscale for separating CO_2 from other gases in flue gas streams [6] as well as in catalytic processes, [7] but have also been used for sampling of environmental CO_2 from atmosphere [8, 9] and soil [8–10].

In microsystems, integration of zeolites has been suggested for applications in microreactors [11–13], micro-preconcentrators [14], separation membranes [13] and gas sensors [15]. The primary methods of zeolite integration are as thin layers, achieved by wash or drop coating using solutions of presynthesised zeolite [11, 13, 15] or in situ growth [11–13]. However, the small amount of material hosted in a thin layer limits adsorption capacity, and a trend towards integration of adsorbents as a bulk material is seen [16]. Mohsen et al. [14] demonstrated integration of zeolite as a bulk material in a micro-preconcentrator by mixing the zeolite with a solvent and pressing it into a prefabricated cavity, but no further analysis of the properties of the material, such as the microstructure, homogeneity and flow resistance, was conducted.

Integration of bulk adsorbents can lead to large pressure drops over the adsorbent material [16]. To overcome this issue on the macroscale, structuring of adsorbents has been explored [17].

To tailor material structure at a small size scale, commonly on the order of 10–100 µm, sacrificial templating can be used. Using this technique, a template, often polymeric or carbon, is added during processing, but then removed after casting, leaving pores behind [18, 19]. Structuring of materials using sacrificial templates is not exclusive to zeolites, but used also for other ceramic materials. To form porous alumina, the use of expandable microspheres has been investigated [20–23]. These spheres consist of a thermoplastic shell housing a gas. Upon heating, the shell softens and the gas expands, causing expansion of the spheres. The spheres can be used as templates in their pre-expanded state, [22, 23] but if the expansion is induced after casting, they can also be used for shaping of complex structures by partly filling a mould and then having the cast filling expand into all details of the mould [20].

This study explores, for the first time, the concept of bulk integration of zeolite in a microsystem through injection of a slurry into a microcavity. Expandable microspheres are used to make the material more permeable by introducing microscopic voids, and to prevent crack formation from the shrinkage occurring upon drying of a slurry in a rigid compartment. To learn how water and microsphere content affect porosity and drying shrinkage, monolithic samples are first prepared and studied. The material is then integrated into microcomponents, and the permeability of the material is evaluated by measuring the flow resistance of these components. In addition, the material's ability to adsorb CO_2 is investigated for future use envisioned in a microfluidic sample handling platform.

MATERIALS AND METHODS

Slurry preparation

Zeolite slurries were prepared from commercially available zeolite 13X powder (average particle size 2 µm, Fluka), together with bentonite powder (Acros Organics), used as inorganic binder, polyethylene glycol (PEG) (MW = 8000, Alfa Aesar), used as sacrificial organic binder, and de-ionized water. Expandable microspheres (Expancel 461 DU 20, Nouryon), with a mean particle size (D_{50}) of 6–9 µm in unexpanded state, were used as a sacrificial templating agent to form voids in the material. According to the manufacturer, expansion of the spheres starts at a temperature of 100–106°C, and the volumetric increase upon heating is up to 60 times the original volume.

Zeolite and bentonite powders were mixed in a mortar. In parallel, PEG was dissolved in water, and this solution added to the powder mixture. All ingredients were mixed by hand in the mortar into a homogeneous slurry without visible agglomerates. For some slurries, microspheres were added followed by additional mixing. Finally, the slurries were loaded into plastic syringes.

Slurries with different water-to-zeolite ratios as well as different contents of microspheres were prepared. The slurries were denoted by the mass of water divided by the total mass before the addition of microspheres, and by the mass of microspheres relative to the mass of zeolite and bentonite, the latter expressed as % dwb (dry weight basis). Four different water ratios were studied: 49.8, 52.2, 54.6 and 57.0 wt%, along with four different ratios of microspheres: 0, 10, 20 and 30 wt% dwb. The mass of bentonite was kept constant at 10 wt% relative to the mass of zeolite, and the mass of PEG was kept constant at 10 wt% relative to the mass of bentonite and zeolite. The compositions of the slurries are detailed in Table 1. From here on, the slurries are referred to as XH$_2$O/YMS, where X represent the water and Y the microsphere ratio, respectively.

Manufacturing of zeolite monoliths

Cylindrical monoliths, used for facilitated material characterization outside of the microcomponents, were cast in polyoxymethylane (POM) moulds (diameter 8 mm, depth 8.6 mm), with removable bottom parts. When possible, slurry was extruded into the mould from the plastic syringe using a 14G (1.6 mm) tapered tip dispensing needle. To reduce the risk of trapping air during casting, the mould was filled from the bottom by inserting the needle tip into the mould. When extrusion through the needle was not possible due to too high viscosity, the slurry was instead extruded from the syringe without a needle. To achieve complete filling of the moulds, they were slightly over-filled and excess slurry removed by scraping with a metal blade.

TABLE 1 Compositions of the slurries by weight.

Water ratio (wt%)	Zeolite (g)	Bentonite (g)	Polyethylene glycol (g)	Water (g)	Microspheres (0/10/20/30 wt% dwb) (g)
49.8	100.0	10.00	11.00	120.0	0/11.00/22.00/33.00
52.2	100.0	10.00	11.00	132.0	0/11.00/22.00/33.00
54.6	100.0	10.00	11.00	145.5	0/11.00/22.00/33.00
57.0	100.0	10.00	11.00	160.5	0/11.00/22.00/33.00

For slurries without and with microspheres, 11 and six samples were cast from each slurry, respectively.

Samples without microspheres were dried under controlled humidity and temperature by placing them along with a beaker of water in a cabinet with adjustable ventilation, which was kept in a climate chamber (ES 250, Finero). Drying conditions, adapted from Akhtar and Bergström [24] were adjusted over a period of 48 h from initial 90% relative humidity (RH) and 35°C to a final 42% RH and 45°C. After this, the samples were placed in a sealed container along with desiccant (silica gel C 2–6 mm, VWR) for final drying.

For samples containing microspheres, the moulds were sealed by clamping a piece of plaster to their top to allow for drying yet restricting the expansion. These moulds were placed in an oven, preheated to 110°C, for 72 h for simultaneous drying and expansion of the spheres.

After drying, the samples were ejected from the moulds by removing the bottom part and gently pushing out the samples using a metal pin. Some samples without expandable spheres were left in their moulds for measurement of the shrinkage. Ejected samples were subject to thermal treatment, adapted from Ojuva et al. [25] and Akhtar and Bergström [24] in a muffle furnace (Thermolyne FB1310M, Thermo Scientific). During the thermal treatment, the temperature was increased at a rate of 1°C min^{-1} to 650°C, and then kept constant for 5 h to allow for complete decomposition and removal of the organic binder and the microspheres. The temperature was then increased at a rate of 5°C min^{-1} to 780°C to increase the mechanical strength of the samples, before they were left to cool to room temperature.

Characterization of zeolite monoliths

The microstructure of the monoliths was studied using a scanning electron microscope (SEM) (LEO1550, Zeiss). Microscopy was performed on cross sections of the monoliths, obtained by carefully cracking them using a scalpel to avoid damages to their original microstructure. Before microscopy, the samples were sputter coated with an approximately 8 nm thick layer of gold-palladium. To obtain a representative view of the monoliths, images of at least 10 randomly selected areas of each sample were captured.

The porosity of the monoliths was determined by Archimedes' principle using a balance (ML 104, Mettler-Toledo) equipped with a density measurement kit (ML DNY 43, Mettler-Toledo). The monoliths were weighed in air before immersed into de-ionized water, where they were left for 28 days to allow for complete intrusion of water into the pores. A wetting agent (Ilford Ilfotol, Ilford Photo) was added to the water at a ratio of 1:200 to promote this. The water-filled monoliths were weighed both in air and immersed in water. Before weighing in air, excess water was carefully removed with a moist tissue.

Similar to as suggested by Engstrand Unosson et al. [26] with an apparent volume determined as described by Ajaxon et al. [27] and assuming a density of water at room temperature of 1.00 g cm^{-3}, the porosity, ϕ, of the samples can be calculated from:

$$\phi = \frac{m_{wet} - m_{dry}}{m_{wet} - m_{im}}, \quad (1)$$

where m_{wet} is the mass of the sample filled with water in air, m_{dry} is the mass of the dry sample, and m_{im} the mass of the sample filled with water in water. The porosity was determined for five monoliths of each slurry, and averaged.

In samples without microspheres, the drying shrinkage causes the top surface of the sample to descend into the mould, leaving an empty overhead space above the sample. Therefore, the shrinkage after drying of these samples was determined by measuring this overhead volume while the samples were still in the mould. The depth profile of the mould top surface and the surface of the sample was obtained with coherence scanning interferometry (CSI) (Nexview NX2, Zygo). From this data, the empty volume was calculated using Matlab (R2018b, MathWorks) after first smoothing the data to interpolate over points were CSI data was missing. The empty volume was then divided by the total volume of the mould. The average shrinkage was determined from five monoliths of each slurry.

Manufacturing of microcomponents

Given that thermal treatment of the cast zeolite slurry requires heating to 780°C, the microcomponents were fabricated from alumina, using High-Temperature Co-fired Ceramics (HTCC) technology. The design of the component (Figure 1), consists of seven layers of 150 µm thick alumina tape (44007-150G, Ferro Corporation), where the middle five layers contain a meandering cavity (width 900 µm, length 19.4 mm), and the top layer the fluidic inlet and outlet

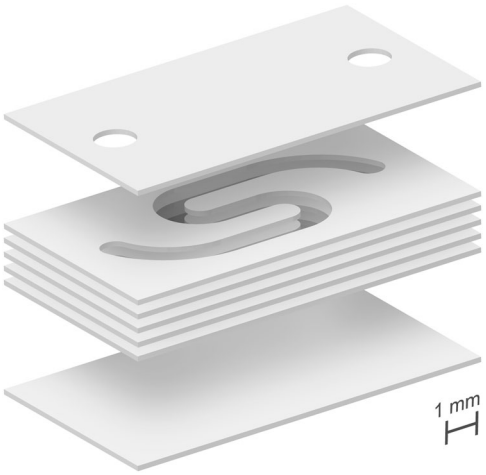

FIGURE 1 Exploded view of the microcomponent showing, bottom up: bottom layer, middle five layers containing the microcavity, and top layer containing fluidic inlet and outlet. Size before sintering.

holes (diameter 1.25 mm). The outer dimensions of the component are 11.3 × 6.00 mm^2. All dimensions given here are before sintering, during which the size is reduced by approximately 15% in all directions.

The five sheets of the cavity stack were placed between two 1 mm thick aluminium plates, packed in a vacuum bag and laminated in an isostatic press at 21 MPa and 70°C for 10 min. The cavity in this stack and the fluidic holes of the top layer were then milled using a printed circuit board plotter (ProtoMat S104, LPKF Laser & Electronics). To support the cavity and holes during the subsequent processing steps, sacrificial graphite material (49000-G, Ferro Corporation) was cut using a laser cutter (AIO G+532 nm, Östling Marking Systems) and manually inserted into the cavities and holes. All tape layers were then laminated in several steps. First, the cavity stack was laminated together with the sacrificial inserts at 3 MPa and 70°C for 10 min to smoothen edges and decrease the height difference between inserts and alumina tapes. The prelaminated cavity stack was then aligned to the top and bottom layers between two 4 mm thick aluminium plates with alignment pins, before another lamination at 3 MPa and 70°C for 10 min took place to make all layers adhere to each other. The stack was then removed from the alignment fixture and placed between the thinner plates before a final lamination at 21 MPa and 70°C for 10 min. From each of the laminates, containing 24 components, individual components were contoured using the plotter, before firing and sintering in a high-temperature furnace (ECF 20/18, Entech). The firing procedure followed a temperature profile suitable for removing the inorganic binders in the ceramic tapes and allowing for complete decomposition and removal of the sacrificial material at temperatures up to 800°C before sintering of the ceramic material at 1550°C for 2 h (Figure 2).

To limit the scope of the study, only four slurry compositions were used for filling of microcomponents: 52.2H_2O/0MS, 52.2H_2O/10MS, 57.0H_2O/10MS and 57.0H_2O/30MS, selected to span a wide porosity range. Six components were filled with each slurry. To evaluate the effect of the added microspheres, three of the slurries contained spheres whereas the fourth did not. The components were filled with slurry using a syringe equipped with a 16G (1.2 mm) tapered tip dispensing needle. The needle tip was pressed onto the fluidic inlet hole on the microcomponent, and slurry was manually injected into the cavity. The components were over-filled to avoid trapping of bubbles, and excess slurry removed using a tissue. The fillings were then dried and thermally treated following the same protocol as for the monolithic samples.

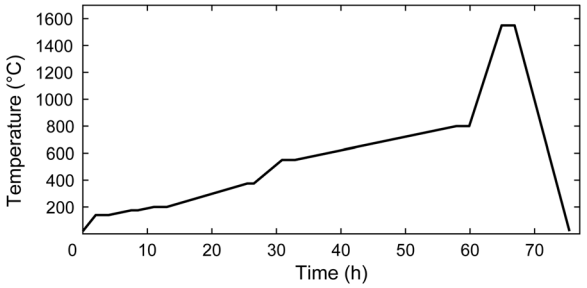

FIGURE 2 Firing profile.

Evaluation of microcomponents

To determine the slurry load, the microcomponents were weighed before and after filling using a balance (XPE206DR, Mettler-Toledo). To study crack formation in the filling, thermally treated components were inspected using X-ray (XTV 130, Nikon).

The permeability of the material, affecting the flow resistance of the microcomponents, was evaluated using a custom-made fluidic setup, in which the components were mounted in an aluminium fixture to which gas-tight fluidic connections were achieved with o-rings. The inlet of the component was open to atmosphere, whereas the outlet was connected to a fluidic system incorporating a flow sensor (AWM1350V, Honeywell) connected to a bench-top multimeter (34450A, Agilent), a pressure sensor (275 Mini-Convectron, Granville-Phillips), and a vacuum pump (EDM6, Edwards High Vacuum) creating a gas flow through the component. To account for leakage in the fluidic system, reference measurements were also performed where the fixture was replaced by a sealed metal tube. Measurements were performed with the component mounted in both possible flow directions, and repeated twice for each component and flow direction. Five components filled with each slurry were evaluated in this way.

Based on these measurements, the flow resistance, R, was calculated from:

$$R = \frac{\Delta p}{q}, \tag{2}$$

where Δp is the pressure difference between the inlet and outlet of the components, and q the measured flow. To exclude the effect of leakage in the system, the final flow resistance of the component, R_C, was given by:

$$\frac{1}{R} = \frac{1}{R_C} + \frac{1}{R_L}, \quad (3)$$

where R_L was the flow resistance from the leakage.

Finally, CO_2 adsorption experiments were conducted employing the principle of temperature swing adsorption, where zeolite adsorbs CO_2 at room temperature, and desorbs it when heated. For these experiments, the microcomponent was mounted in a fixture made from aluminium and printed circuit board, and gas-tight connections between component and fixture were again achieved using o-rings. The outlet of the component was connected to a microplasma spectrometer (Pithos, Fourth State Systems) through a capillary (inner diameter 75 µm, length 2 cm), used to adjust the pressure in, and flow through, the spectrometer. The component was fed with a gas mixture of about 20% CO_2 in N_2, mixed from pure gases in a 100 mL glass syringe. Adsorption and desorption of CO_2 were achieved by altering the temperature of the component between room temperature and 140°C using a hot plate. Before being mounted, the components had been dehydrated in an oven at 140°C for at least 24 h. These experiments were conducted on a total of four microcomponents, one filled with each slurry.

RESULTS

Characterization of monoliths

All slurries except the most viscous one, with 49.8H_2O/30MS, were possible to extrude through the needle. All samples containing microspheres expanded enough to compensate for the volumetric loss upon drying, so that the moulds remained completely filled. In fact, the expansion was even larger than required to keep the moulds filled, making the slurry expand out of the mould during drying and expansion, since the seal between the plaster plate and the mould was not completely tight.

The dried monoliths were fragile, and submillimetre sized fragments detached during ejection from the moulds. For monoliths without microspheres, this problem was more prominent, and several of these monoliths fractured into pieces on release. After thermal treatment at 780°C, the samples were stable enough to allow careful handling during subsequent testing, even though some further detachment of small fragments did occur.

SEM inspection (Figure 3) revealed spherical voids in samples cast from slurries containing microspheres. However, the voids were not evenly distributed throughout the material. Qualitative inspection of all images captured revealed that the overall amount of voids increased with sphere content and that there was no difference in microstructure between materials with the same amount of microspheres but different water contents.

Porosities, as calculated from Equation (1), spanning from 55% to 72%, were obtained for the different slurry compositions (Figure 4). For monoliths with similar amount of water, the porosity increases with microsphere content. For monoliths with similar amount of microspheres, there was a general trend of porosity increasing with water content, even though two samples deviated from this trend. One of the monoliths of 54.6H_2O/0MS was found to have an exceptionally high porosity, which cause was identified as an experimental error, wherefore this sample was considered an outlier in further analysis. Most monoliths experienced some kind of fragmentation during water intrusion, so that pieces of varying size detached from them. As much of the original monolith and the detached pieces as possible was used for weighing. Four of the 49.8H_2O/0MS monoliths disintegrated into small pieces during water intrusion and had to be excluded from further measurements.

The shrinkage after drying of monoliths without microspheres increased with water content, spanning from 6% to 14% (Figure 5).

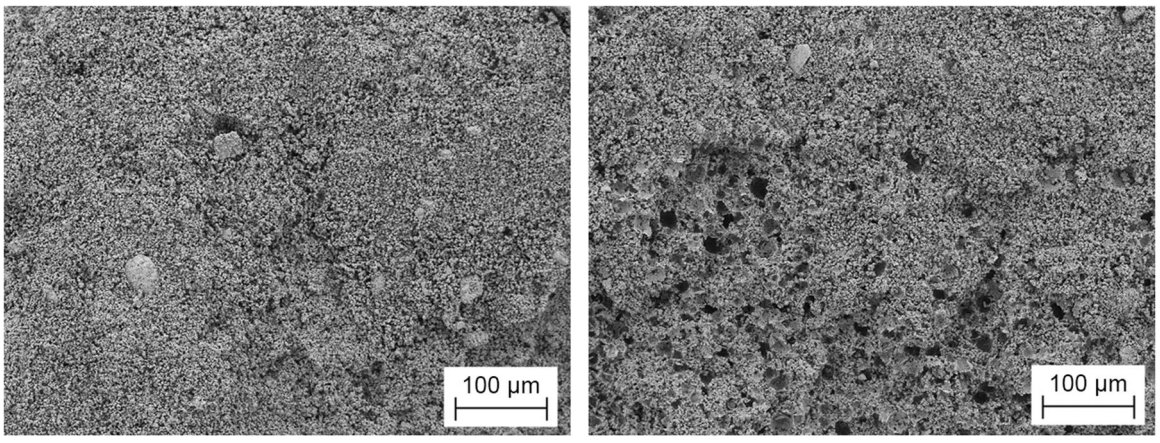

FIGURE 3 Scanning electron microscope images showing the microstructures of samples cast from a slurry without microspheres (left) and a slurry with 20 wt% microspheres (right). Unevenly distributed spherical voids are seen in the sample cast from the slurry with microspheres. Both slurries had the same water content, 52.2 wt%, and both images are at the same magnification.

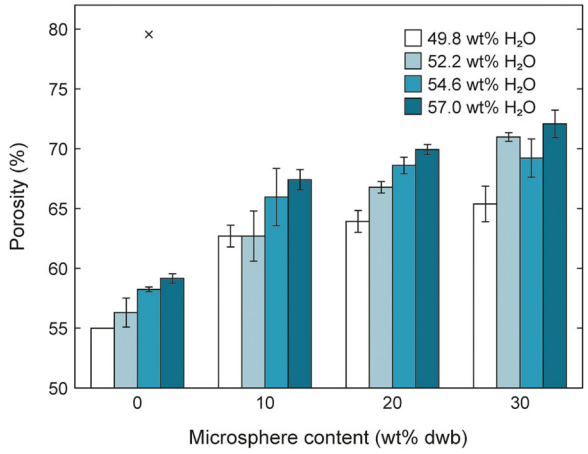

FIGURE 4 Porosity of monoliths made from different slurry compositions, grouped by microsphere content. Error bars represent standard deviation. 'x' marks an outlier due to measurement error. The number of samples was five for all slurries, except for 54.6H_2O/0MS, where it was four, and 49.8H_2O/0MS, where only one sample was used and hence standard deviation is missing.

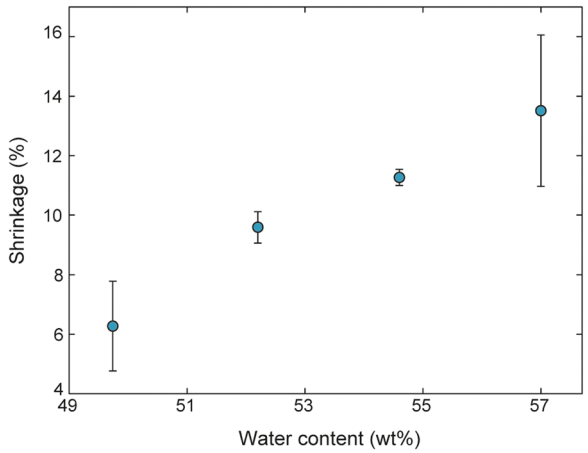

FIGURE 5 Shrinkage after drying of monoliths without microspheres. Error bars represent standard deviation. The number of samples was five for all water contents.

Evaluation of microcomponents

All slurries with 49.8 wt% H_2O, as well as slurries with 52.2 wt% H_2O and a microsphere content of 20 wt% dwb or more, were too viscous to be used for filling, whereas all other slurries were useable. The weights of the zeolite fillings are presented in Table 2. For 57.0H_2O/30MS, one sample had a trapped air bubble and was therefore regarded as an outlier.

During visual inspection of the filled and thermally treated microcomponents, a dark shadow was seen at the top and bottom of the components, following the outline of the microcavity.

X-ray inspection (Figure 6) revealed that large cracks were present in all fillings without microspheres. For fillings with microspheres, only some fine cracks could be distinguished. These fine cracks were most prominent in the components filled with 57.0H_2O/30MS. Fewer fine cracks were seen in components filled with 57.0H_2O/10MS, whereas no cracks at all could be seen in components filled with 52.2H_2O/10MS.

TABLE 2 Average and standard deviation of the zeolite filling weights in the microcomponents after thermal treatment.

Slurry used for filling	Average filling weight (mg)
52.2H_2O/0MS	4.63 ± 0.04
52.2H_2O/10MS	4.42 ± 0.06
57.0H_2O/10MS	3.49 ± 0.06
57.0H_2O/30MS	3.81 ± 0.09

Note: The number of samples was six for each slurry, except for 57.0H_2O/30MS were an outlier has been excluded.

The flow resistance of all components, calculated according to Equation (3) and averaged over the four measurements conducted on each component, is presented in Figure 7. The five out of six samples used during the measurements were randomly selected, except for 57.0H_2O/30MS where the outlier with a bubble was excluded. Flow resistance from leakage was 1157 kPa min cm^{-3}, determined as the average of two measurements (R_L = 1335 and 980 kPa min cm^{-3}, respectively).

Figure 8 shows the CO_2 signal from the spectrometer during the adsorption experiment for the sample containing slurry 52.2H_2O/10MS. At the beginning of the measurement, the component was heated to 140°C, and gas containing 20% CO_2 was flowing through the component without being adsorbed. At t = 90 s, the component was cooled to room temperature, and adsorption of CO_2 in the zeolite material started, resulting in a sudden drop in CO_2 concentration until the zeolite material was completely filled with CO_2 after an additional 200 s. At t = 400 s, the component was heated again, and the CO_2 adsorbed in the zeolite material was desorbed over a period of about 60 s, resulting in a peak in CO_2 concentration in the spectrometer. This procedure was then repeated. Components filled with all four different slurries were seen to adsorb and desorb CO_2 in this way, although the amplitude of the signal varied largely between components.

DISCUSSION

Characterization of monoliths

In this work, porosities between 55% and 72% were obtained. However, zeolite 13X is hygroscopic, and the measured dry mass of the monolithic samples, used to calculate porosity, includes the mass of water adsorbed in the material. Hence, the true porosity of the monoliths is probably larger than that measured here. In addition, the fragmentation of samples that occurred during water intrusion also contributed to a reduction in the measured porosity, since parts of the samples that were included in the dry mass were missing in the subsequent measurements.

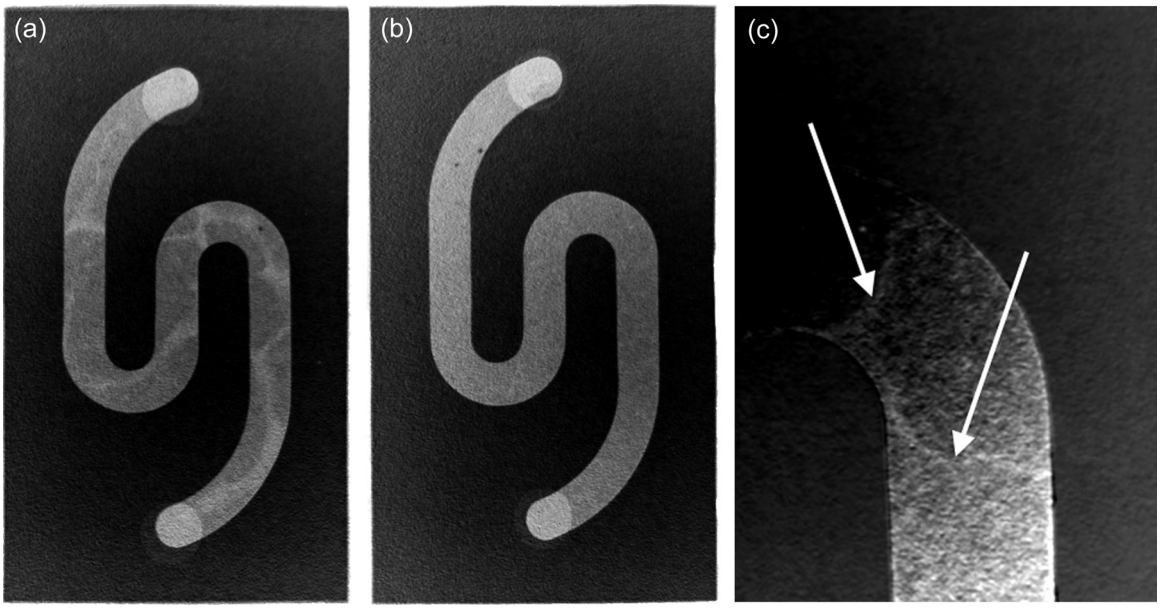

FIGURE 6 X-ray images of microcomponents filled with different slurries. The lack of microspheres in 52.2H_2O/0MS causes a clear crack pattern (a), whereas a filling free from cracks is seen for 52.2H_2O/10MS (b). Fine cracks (highlighted with arrows) are revealed at higher magnification, here in a component filled with 57.0H_2O/30MS (c).

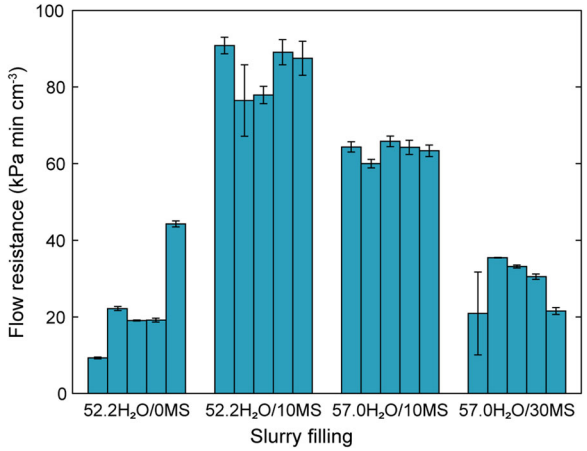

FIGURE 7 Average flow resistance for all microcomponents, grouped by the slurry used for filling. Four measurements were conducted on each component. Error bars represent standard deviation.

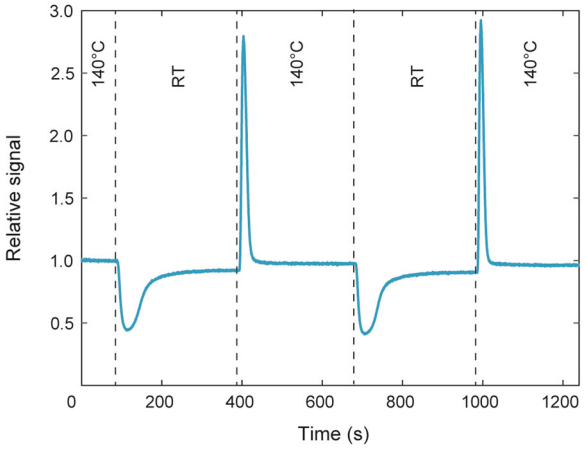

FIGURE 8 CO_2 signal from adsorption experiment on a microcomponent filled with 52.2H_2O/10MS. *Y*-axis presents signal from the spectrometer relative to the signal at measurement start, where CO_2 concentration is 20%. During the experiment, the temperature of the component is altered between room temperature and 140°C, as indicated by the dashed lines, causing adsorption and desorption of CO_2 in the zeolite filling, respectively.

The microstructure of the monoliths (Figure 3) was inhomogeneous. This indicates that the final mixing of the slurries after addition of microspheres was not sufficient. Ways of overcoming this problem could include more thorough mechanical mixing, use of a dispersant, or surface treatment of the microspheres.

In measurements of the shrinkage (Figure 5), the standard deviations are large for samples with the smallest and the largest water fractions. For samples with the smallest water fraction, this can possibly be attributed to the higher viscosity of these samples, since the high viscosity increases the risk of entrapment of air in the sample. The CSI measurement only mapped the top surface of the samples; hence, it cannot account for any voids inside the sample. The large standard deviation for samples with the largest water fraction is a result of one sample showing an exceptionally small shrinkage of 9.13%.

Integration in microcomponents

When fillings without microspheres were used, crack formation from the shrinkage upon drying was confirmed through X-ray imaging.

However, for fillings containing microspheres, this shrinkage was compensated for by the expansion of the spheres, and no major cracks were seen. This is important to obtain a homogeneous gas flow through the filling, which enhances adsorption.

The fine cracks seen in 57.0H_2O/10MS and 57.0H_2O/30MS fillings (Figure 6) is possibly a result of either the material expanding too much to retain structural stability, or because of the drying and sphere expansion not being synchronized. In the monoliths, the timing appeared good, but since water transport during drying is different in a long and narrow channel compared to the cylindrical mould, some adjustment of the drying conditions might be necessary for the microcomponents. No fine cracks were seen for 52.2H_2O/10MS fillings, probably because of the lower porosity of this filling, and, hence, the smaller effects from shrinkage and expansion.

The sphere content caused sufficient expansion to enable complete filling of the microcavity in all cases, even for 57.0H_2O/10MS that contained the largest amount of water in combination with the smallest amount of microspheres. Thus, even the smallest amount of microspheres was enough to compensate for the shrinkage of 14% seen in Figure 5. In addition, this filling had the lowest viscosity, which is advantageous for filling of cavities with small dimensions or complex shape.

Flow resistance

In the measurement of the flow resistance (Figure 7), two components, one filled with 52.2H_2O/10MS and one with 57.0H_2O/30MS, have particularly large standard deviation. This is a result of a large difference in flow resistance depending of the flow direction, hence the mounting, of these components (20% and 65% difference, respectively), probably due to defects around the fluidic outlets of the components, causing leakage between the component and the o-ring. Hence, the higher of the measured values for these components can be assumed to be closer to reality. For all other components, the difference in flow resistance between mounting directions was less than 5%. If the above-mentioned samples are ignored, there is a trend of increased standard deviation when flow resistance increases, probably due to increasing uncertainties in the sensors at low pressure and flow. In addition, the effects of leakages in the fluidic setup becomes more prominent at higher flow resistances.

The flow through the microcomponents under the conditions of this study can be assumed to be laminar. For such a flow in a straight tube with circular cross section of radius r and length L the flow resistance, R, in the tube can be calculated from:

$$R = \frac{8\eta L}{\pi r^4}, \tag{4}$$

where η is the viscosity of the flowing gas. Using the cavity length of 16.5 mm after sintering and a viscosity of air of 18.4 µPa s at 25°C, calculated according to McInally, [28] the flow resistance of the components is equivalent to that of a tube of the same length with a radius of about 20–30 µm.

Assuming that the porosity of a filling is the same as for monolithic samples made from the same slurry, flow resistance and porosity should correlate as presented in Figure 9. For fillings containing microspheres, the flow resistance decreases with increasing porosity. The relationship looks linear, but according to the Ergun equation [29] and Equation (2), for laminar flow, the flow resistance, R, is related to the fractional porosity, ϕ, as:

$$R \propto \frac{(1-\phi)^2}{\phi^3}. \tag{5}$$

Hence, the increase in flow resistance should be more rapid the lower the porosity becomes. However, the relationship might look linear here due to the narrow porosity range.

Components filled with slurry without microspheres, that is, the material shown to have the lowest net porosity from the study of the monoliths, exhibited the lowest flow resistance. The explanation is that, although the material's permeability is governed by its porosity, the flow resistance of a component depends also on the presence of cracks, like those resulting from drying. Had the filling been free from cracks, the flow resistance would be expected to be much higher than what is seen in Figure 9, and also correlate better with porosity. Finally, the quite large standard deviation for the fillings without microspheres is likely because of the inhomogeneous cracking pattern in these fillings, where unevenly distributed cracks along the length of the cavity provided open paths for the flow that influenced the net flow resistance.

Due to the open paths, most of the gas flow in components with cracks is probably located to the cracks, whereas in components with evenly distributed fillings, the gas flow is more uniformly spread across the cross-section of the cavity. This affects the adsorptive properties of the zeolite material, since when cracks are present, only a small part of the zeolite is exposed to the main gas flow in the cracks, and mass

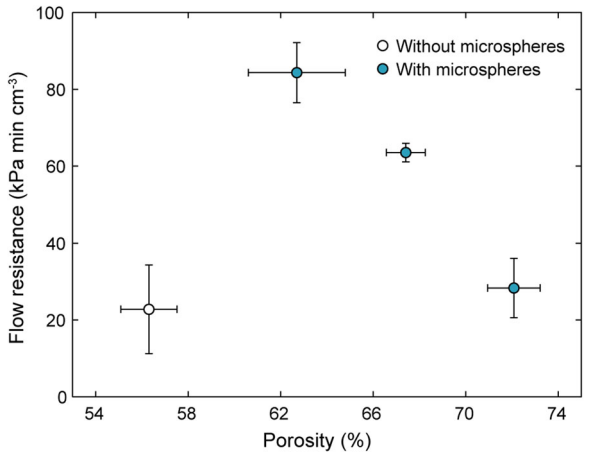

FIGURE 9 Flow resistance, calculated as the average of the 20 measurements made on components filled with the same slurry, versus the porosity of the corresponding monolith. A trend of decreasing flow resistance with increased porosity is seen for components filled with slurries containing microspheres (filled markers). Error bars represent standard deviation.

transfer through slow diffusion in the material then severely limits the adsorption process.

CO_2 adsorption

The adsorption experiments confirmed that all the processed zeolite fillings could adsorb and desorb CO_2. However, these experiments also suffered from compatibility issues between components and the spectrometer. The microplasma source in the spectrometer has an operation pressure between 1 and 1000 Pa. When analysing samples at atmospheric pressure, the pressure is reduced using a fine capillary between the sample and the spectrometer. According to Equation (4), the capillary used in this study has a flow resistance of about 8 kPa min cm^{-3}, that is, on the same or lower order of magnitude than the components. However, to use the full adsorption capacity of the zeolite material, the pressure drop over the component should be as small as possible, since reduced pressure reduces the adsorption capacity. If the pressure drop over the component should be considered negligible, the capillary should have a flow resistance at least ten times larger than the component. However, such a large flow resistance would have reduced the operating pressure in the spectrometer below its functional range. It could be possible to increase the pressure in the plasma by reducing the pump efficiency, but this would result in a very low flow rate through the plasma and, hence, long measurement times.

So, to use the spectrometer there had to be a considerable pressure drop along the length of the cavity, which reduced the possible adsorption capacity of the material. In addition, since the flow resistance varies between components, so does the pressure drop, making the adsorption conditions vary. Therefore, it is not possible to determine how much of the adsorption capacity that might have been lost compared to the unprocessed zeolite or to make reliable relative comparisons between the components.

In Figure 8, there is a difference in signal corresponding to 20% CO_2 at room temperature and 140°C. This is also a consequence of the relatively large flow resistance of the component explained by the fact that the viscosity of a gas increases with temperature, hence the flow resistance increases with temperature according to Equation (4).

Outlook

The results of this study demonstrate the feasibility of integrating zeolite as a bulk material in a microcomponent. Compared to the more common microcomponent integration strategy, as thin layers, the bulk material is beneficial due to its larger adsorption capacity. However, the adsorption capacity could not be determined here due to compatibility issues with the spectrometer used. To make the microcomponents compatible with the spectrometer in the intended application, their flow resistance needs to be reduced. This can be accomplished by changing the design, for example, by increasing the cross section of the cavity or using several cavities in parallel, or by further increasing the porosity of the material. If the latter is chosen, it would also be of interest to investigate how much the porosity can be increased before the mechanical stability is lost. Reducing the flow resistance of the components by one or more of the above methods might also help to avoid the dark discolorations seen after thermal treatment of the filled microcomponents, since these are probably due to incomplete transportation of the decomposed organic materials in the filling in the long and narrow channel.

Future work on the microcomponents towards their use in the intended application also includes integration of a heater and a temperature sensor, forming an entire microsystem. Looking at the complete microfluidic platform suggested here, other parts are needed to fulfil the requirements of the whole sample handling procedure. For example, since zeolite is hygroscopic, any water contained in the sample to be analysed needs to be removed before introducing the sample to the component presented here. In addition, if the sample is liquid, a module that separates gas from liquid is required. However, the initial results presented in this study indicate that the use of a microfluidic platform is a viable way towards simpler and less expensive measurements of environmental CO_2.

CONCLUSIONS

In this study, structured zeolite 13X materials were integrated into ceramic microcomponents by injection of zeolite slurry into a microcavity. The materials were integrated in bulk form, which has the potential of larger adsorption capacities compared to the more commonly seen integration as thin layers.

- Addition of expandable microspheres to the slurry reduced crack formation in the integrated material by countering drying shrinkage.
- Complete fillings free from cracks were achieved, which is of great importance for well-distributed gas flow and enhanced adsorption in the component.
- By varying the amount of water and microspheres in the slurry, it was possible to structure the zeolite material and tune its porosity between 55% and 72%.
- The porosity was seen to affect the flow resistance of the microcomponents, where increasing the porosity of the filling in the microcomponents from 62% to 72% reduced the flow resistance from 84 to 28 kPa min cm^{-3}.
- Zeolite materials integrated in the microcomponents were seen to retain their ability to adsorb CO_2 after processing.

To summarize, this indicates that the integrated material has potential for use in a microsystem for sampling of environmental CO_2, which will contribute to making measurements of greenhouse gases simpler, less expensive and hence more available.

ACKNOWLEDGEMENTS

The Knut and Alice Wallenberg Foundation is acknowledged for funding the cleanroom facilities. Hans Östling and Expancel,

Sundsvall, are acknowledged for kindly providing the expandable microspheres. Dan Åkerfeldt is acknowledged for help with design and fabrication of moulds and fixtures. This project has received funding from Formas (No. 2016-00706).

CONFLICT OF INTEREST STATEMENT

The authors declare no conflict of interest.

DATA AVAILABILITY STATEMENT

The data that support the findings of this study are available from the corresponding author upon reasonable request.

ORCID

Erika Åkerfeldt http://orcid.org/0000-0003-1215-8633
Greger Thornell http://orcid.org/0000-0003-4468-6801
Anders Persson http://orcid.org/0000-0003-2853-9238

REFERENCES

[1] P. Friedlingstein, M. O'Sullivan, M. W. Jones, R. M. Andrew, L. Gregor, J. Hauck, C. Le Quéré, I. T. Luijkx, A. Olsen, G. P. Peters, W. Peters, J. Pongratz, C. Schwingshackl, S. Sitch, J. G. Canadell, P. Ciais, R. B. Jackson, S. R. Alin, R. Alkama, A. Arneth, V. K. Arora, N. R. Bates, M. Becker, N. Bellouin, H. C. Bittig, L. Bopp, F. Chevallier, L. P. Chini, M. Cronin, W. Evans, S. Falk, R. A. Feely, T. Gasser, M. Gehlen, T. Gkritzalis, L. Gloege, G. Grassi, N. Gruber, Ö. Gürses, I. Harris, M. Hefner, R. A. Houghton, G. C. Hurtt, Y. Iida, T. Ilyina, A. K. Jain, A. Jersild, K. Kadono, E. Kato, D. Kennedy, K. Klein Goldewijk, J. Knauer, J. I. Korsbakken, P. Landschützer, N. Lefèvre, K. Lindsay, J. Liu, Z. Liu, G. Marland, N. Mayot, M. J. McGrath, N. Metzl, N. M. Monacci, D. R. Munro, S. I. Nakaoka, Y. Niwa, K. O'Brien, T. Ono, P. I. Palmer, N. Pan, D. Pierrot, K. Pocock, B. Poulter, L. Resplandy, E. Robertson, C. Rödenbeck, C. Rodriguez, T. M. Rosan, J. Schwinger, R. Séférian, J. D. Shutler, I. Skjelvan, T. Steinhoff, Q. Sun, A. J. Sutton, C. Sweeney, S. Takao, T. Tanhua, P. P. Tans, X. Tian, H. Tian, B. Tilbrook, H. Tsujino, F. Tubiello, G. R. van der Werf, A. P. Walker, R. Wanninkhof, C. Whitehead, A. Willstrand Wranne, R. Wright, W. Yuan, C. Yue, X. Yue, S. Zaehle, J. Zeng, B. Zheng, *Earth Syst. Sci. Data* **2022**, *14*(11), 4811. https://doi.org/10.5194/essd-14-4811-2022

[2] D. Bastviken, J. Wilk, N. T. Duc, M. Gålfalk, M. Karlson, T. S. Neset, T. Opach, A. Enrich-Prast, I. Sundgren, *Environ. Res. Lett.* **2022**, *17*(10), 104009. https://doi.org/10.1088/1748-9326/ac8fa9

[3] D. Bastviken, I. Sundgren, S. Natchimuthu, H. Reyier, M. Gålfalk, *Biogeosciences* **2015**, *12*(12), 3849. https://doi.org/10.5194/bg-12-3849-2015

[4] *Microsystems and Nanotechnology* (Eds: Z. Zhou, Z. Wang, L. Lin), Springer, Berlin, Heidelberg, **2012**.

[5] A. Persson, M. Berglund, *J. Appl. Phys.* **2020**, *127*, 064502. https://doi.org/10.1063/1.5134947

[6] M. Karimi, M. Shirzad, J. A. C. Silva, A. E. Rodrigues, *Environ. Chem. Lett.* **2023**, *21*(4), 2041. https://doi.org/10.1007/s10311-023-01589-z

[7] J. Liang, Z. Liang, R. Zou, Y. Zhao, *Adv. Mater.* **2017**, *29*(30), 1701139. https://doi.org/10.1002/adma.201701139

[8] P. Cheng, S. Wu, Y. Fu, X. Xiong, Z. Niu, Y. Fan, *Radiocarbon* **2017**, *59*(2), 281. https://doi.org/10.1017/RDC.2016.103

[9] P. Ascough, N. Bompard, M. H. Garnett, P. Gulliver, C. Murray, J. A. Newton, C. Taylor, *Radiocarbon* **2024**. https://doi.org/10.1017/RDC.2024.9

[10] M. H. Garnett, I. P. Hartley, D. W. Hopkins, M. Sommerkorn, P. A. Wookey, *Soil Biol. Biochem.* **2009**, *41*(7), 1450. https://doi.org/10.1016/j.soilbio.2009.03.024

[11] L. A. Truter, V. Ordomsky, J. C. Schouten, T. A. Nijhuis, *Microporous Mesoporous Mater.* **2016**, *226*, 424. https://doi.org/10.1016/j.micromeso.2016.02.016

[12] G. Zhang, X. Zhang, J. Lv, H. Liu, J. Qiu, K. L. Yeung, *Catal. Today* **2012**, *193*(1), 221. https://doi.org/10.1016/j.micromeso.2016.02.016

[13] Y. S. S. Wan, J. L. H. Chau, A. Gavriilidis, K. L. Yeung, *Microporous Mesoporous Mater.* **2001**, *42*(2), 157. https://doi.org/10.1016/S1387-1811(00)00332-2

[14] Y. Mohsen, H. Lahlou, J. B. Sanchez, F. Berger, I. Bezverkhyy, G. Weber, J. P. Bellat, *Microchem. J.* **2014**, *114*, 48. https://doi.org/10.1016/j.microc.2013.12.001

[15] M. Denoual, D. Robbes, S. Inoue, Y. Mita, J. Grand, H. Awala, S. Mintova, *Sens. Actuat. B* **2017**, *245*, 179. https://doi.org/10.1016/j.snb.2017.01.131

[16] I. Lara-Ibeas, A. Rodríguez Cuevas, S. le Calvé, *Sens. Actuat. B* **2021**, *346*, 130449. https://doi.org/10.1016/j.snb.2021.130449

[17] F. Rezaei, P. Webley, *Chem. Eng. Sci.* **2009**, *64*(24), 5182. https://doi.org/10.1016/j.ces.2009.08.029

[18] Y. Chen, N. Wang, O. Ola, Y. Xia, Y. Zhu, *Mater. Sci. Eng. R Rep.* **2021**, *143*, 100589. https://doi.org/10.1016/j.mser.2020.100589

[19] J. D. G. Rocha, D. L. P. Macuvele, C. J. Andrade, H. G. Riella, N. Padoin, C. Soares, *J. Environ. Chem. Eng.* **2023**, *11*, 109397. https://doi.org/10.1016/j.jece.2023.109397

[20] L. Andersson, L. Bergström, *J. Eur. Ceram. Soc.* **2008**, *28*(15), 2815. https://doi.org/10.1016/j.jeurceramsoc.2008.04.020

[21] L. Andersson, A. C. Jones, M. A. Knackstedt, L. Bergström, *Acta Mater.* **2011**, *59*(3), 1239. https://doi.org/10.1016/j.actamat.2010.10.056

[22] S. Hooshmand, J. Nordin, F. Akhtar, *Int. J. Ceramic Eng. Sci.* **2019**, *1*(2), 77. https://doi.org/10.1002/ces2.10013

[23] M. Ciurans Oset, J. Nordin, F. Akhtar, *Ceramics* **2018**, *1*(2), 329. https://doi.org/10.3390/ceramics1020026

[24] F. Akhtar, L. Bergström, *J. Am. Ceram. Soc.* **2011**, *94*(1), 92. https://doi.org/10.1111/j.1551-2916.2010.04044.x

[25] A. Ojuva, F. Akhtar, A. P. Tomsia, L. Bergström, *ACS Appl. Mater. Interfaces* **2013**, *5*(7), 2669. https://doi.org/10.1021/am400122r

[26] J. Engstrand Unosson, C. Persson, H. Engqvist, *J. Biomed. Mater. Res. Part B Appl. Biomater.* **2015**, *103*(1), 62. https://doi.org/10.1002/jbm.b.33173

[27] I. Ajaxon, Y. Maazouz, M. P. Ginebra, C. Öhman, C. Persson, *J. Biomater. Appl.* **2015**, *30*(5), 526. https://doi.org/10.1177/0885328215594293

[28] M. McInally, *Am. J. Phys.* **1963**, *31*(9), 732. https://doi.org/10.1119/1.1969796

[29] S. Ergun, *Chem. Eng. Prog.* **1952**, *48*(2), 89.

How to cite this article: E. Åkerfeldt, G. Thornell, A. Persson, *Appl. Res.* **2024**;3:e202300105. https://doi.org/10.1002/appl.202300105